Probing molecular frame photoelectron angular distributions via high-order harmonic generation from aligned molecules

2012 J. Phys. B: At. Mol. Opt. Phys. 45 194010

(http://iopscience.iop.org/0953-4075/45/19/194010)

J. Phys. B: At. Mol. Opt. Phys. **45** (2012) 194010 (9pp) doi:10.1088/0953-4075/45/19/194010

Probing molecular frame photoelectron angular distributions via high-order harmonic generation from aligned molecules

C D Lin[1], Cheng Jin[1], Anh-Thu Le[1] and R R Lucchese[2]

[1] J R Macdonald Laboratory, Physics Department, Kansas State University, Manhattan, KS 66506-2604, USA
[2] Department of Chemistry, Texas A&M University, College Station, TX 77843-3255, USA

E-mail: cdlin@phys.ksu.edu

Received 25 April 2012, in final form 25 June 2012
Published 24 September 2012
Online at stacks.iop.org/JPhysB/45/194010

Abstract
We analyse the theory of single photoionization (PI) and high-order harmonic generation (HHG) by intense lasers from aligned molecules. We show that molecular-frame photoelectron angular distributions can be extracted from these measurements. We also show that, under favourable conditions, the phase of PI transition dipole matrix elements can be extracted from the HHG spectra. Furthermore, by varying the polarization axis of the HHG generating laser with respect to the polarization axis of the aligning laser, it is possible to extract angle-dependent tunnelling ionization rates for different subshells of the molecules.

(Some figures may appear in colour only in the online journal)

1. Introduction

Photoionization (PI) is one of the most basic tools for studying the structure of molecules. Experimentally, measurements of total, partial and differential PI cross sections (PICS) of molecules have a long history [1]. With the availability of synchrotron radiation light sources in the last few decades, PICS of many molecules have been investigated over a broad energy region with ever-improving resolution. Meanwhile, multi-parameter coincidence experiments have further allowed the disentanglement of the different fragmentation channels [2]. However, most of the experiments have been carried out from an ensemble of randomly oriented molecules; thus, the rich structure of the molecular-frame photoelectron angular distributions (MFPAD) for fixed-in-space molecules predicted in the seminal paper by Dill [3] more than 35 years ago remains largely unexplored. In recent years, using high-energy XUV or x-ray photons, fixed-in-space PI has been investigated by using photoelectron–photoion coincidence techniques [4–6]. Such experiments require that an electron be removed from the inner orbital of a molecule and the molecular ion dissociates after photoabsorption. If the dissociation time is short compared to the rotational period of the ion, then the direction of the molecular axis at the time of dissociation can be inferred from the direction of the recoil of the ion fragments. Clearly, this method is not generally applicable to the most interesting outer-shell PI and not for all molecules of interest.

Molecules in free space in general are randomly distributed. The development of techniques to align or orient molecules has always been an important goal of chemical reaction dynamics [7]. Methods based on collisional processes (such as in a buffer gas) or static electric fields have been used [8, 9], but the achievable density often is too low to be suitable as targets for PI studies. In recent years, it has been shown that molecules can be aligned by an intense linearly polarized laser field or by other optical means [7]. If the durations of these pulses are shorter than the typical rotational period of the molecules, then molecules can be impulsively aligned, in that they are periodically aligned after the pulse is over. These field-free alignments are maintained over a duration of tens to hundreds of femtoseconds, during which these aligned molecules can be probed by different means. Ideally, these aligned molecules would be exposed to synchrotron radiation, from which molecular frame PI can be investigated. However,

typical light pulses from synchrotron radiation sources have durations of hundreds of picoseconds. Synchronization with several kilohertz laser pulses is also not easy to accomplish. An alternative possibility is to use XUV lights from high-order harmonics generated by the same laser that is used to orient/align the molecules. However, the fluence of these high harmonics is still too feeble. The first such experiment measured the total ion yields [10] only. Photoelectron angular distribution measurements are beginning to appear, but the degree of alignment and the electron energy resolution are still limited [11–13].

In this paper, we address the probing of MFPAD via high-order harmonic generation (HHG) from aligned molecules. Typically, molecules are impulsively aligned by a long 800 nm laser pulse with duration of the order of 100 fs, and intensity of a few times of 10^{13} W cm^{-2}. The high harmonics are generated by a more intense 'probe laser', or HHG driving laser, at a time delay when the molecules are maximally aligned (or anti-aligned). The relative polarization between the two laser pulses can be adjusted by a rotatable wave plate. The wavelength of the probe pulse used is normally the same 800 nm laser. In recent years, however, near-infrared (NIR) lasers with wavelength up to 1800 nm from high-energy optical parametric amplifiers have been used to generate harmonics [14–16]. With NIR lasers the photon spectra extend to a much broader energy range, scaling roughly proportional to the square of the laser wavelength.

The basic mechanism of HHG has been well understood since the 1990s [17]. According to the three-step model, when a molecule is exposed to an intense laser pulse, an electron that was released earlier through tunnelling ionization may be driven back by the oscillating electric field of the laser to recollide with the parent molecular ion. High-order harmonics are emitted when the returning electrons recombine with the parent ion. This last step is a photorecombination (PR) process, which is the inverse of PI and the two share the same transition dipole matrix element. For years, the three-step model has been serving as a qualitative tool for the interpretation of the HHG process. Recently, this model has been recast in a quantitative rescattering (QRS) theory where the relation between HHG and the transition dipole matrix elements has been explicitly established [18–20]. Thus, it appears that it is straightforward to extract PI information from the HHG spectra. However, experimentally high harmonics are generated coherently from all the induced dipoles of the molecules inside the focal volume of the laser. Since the intense laser pulse and the harmonics co-propagate in the medium, the fields may be modified, and the harmonics depend critically on the phase matching between these emitting dipoles [21, 22]. Thus, the HHG spectra observed in the laboratory in general depend on the focusing condition, gas pressure, gas jet length, spatial profiles of the laser pulse and how and where the harmonics are collected. With such complications, can one still extract PI information of individual molecules from the measured macroscopic HHG spectra? Various aspects of this issue have been addressed in a number of publications from our group in recent years. While a detailed review on this topic before 2010 could be found in [20], direct comparison with experimental HHG spectra based on QRS theory has been carried out only in the last two years. In this contribution, we offer a self-contained full description on how the experimental HHG spectra are calculated based on QRS theory and how the propagation of harmonics in the medium can affect the observed spectra. Through specific examples from N_2 molecules, we wish to convey the intricate relation between the observed HHG spectra and the elementary PI processes of single molecules. We wish to clarify the intrinsic limitations of the three-step model, as well as the tomography procedure where HHG spectra were used to 'retrieve' the ground state wavefunctions of the molecules [23–25, 16].

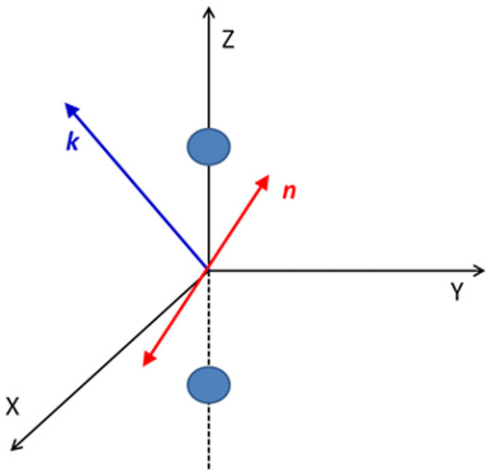

Figure 1. Sketch of photoelectron emission in the molecular frame, where **k** is the momentum vector of the photoelectron, **n** is the direction of the light polarization.

The rest of this paper is organized as follows. First we summarize the recently developed QRS theory that relates the HHG spectra generated from individual molecules with the transition dipole matrix elements in the PI (or PR) cross sections. Using N_2 as an example, we draw the connection between the MFPAD with the HHG spectra from aligned molecules. We then discuss the effect of propagation of the harmonics in the medium. We will address experimental conditions where transition dipole matrix elements (magnitude and phase) can be extracted, thus yielding MFPAD.

2. Photoionization and high-order harmonic generation

2.1. Basic equations for photoionization of molecules

The general expression for the calculation of doubly differential photoionization cross section (DPICS) is given by

$$\frac{\mathrm{d}^2\sigma^I}{\mathrm{d}\Omega_{\hat{k}}\mathrm{d}\Omega_{\hat{n}}} = \frac{4\pi^2\omega k}{c}\left|\left\langle\Psi_i|\vec{r}\cdot\hat{n}|\Psi_{f,\vec{k}}^{(-)}\right\rangle\right|^2, \qquad (1)$$

where $\vec{k}$ is the momentum vector of the photoelectron, $\hat{n}$ is the direction of the polarization of the light, ω is the energy of the photon which is given by the sum of the kinetic energy of the photoelectron and the ionization potential of the specific subshell from which the electron was removed and c is the speed of light. Figure 1 depicts these vectors

for a molecule fixed in space along the laboratory Z-axis. Atomic units are used throughout this paper unless otherwise indicated. The transition dipole matrix is between the initial state wavefunction $|\Psi_i\rangle$ and incoming continuum final-state wavefuction $\left|\Psi^{(-)}_{f,\vec{k}}\right\rangle$. The matrix element has been written in the single particle form, but in general multi-electron wavefunctions are used in the calculation. The calculation of the dipole transition matrix elements follows the prescription and the computer codes developed by one of us [26]. The initial state wavefunction is obtained from the MOLPRO code [27], and the continuum wavefunction is calculated using the Schwinger variational method [26]. Since PR is an inverse process of PI, the differential cross section is given by

$$\frac{\mathrm{d}^2\sigma^R}{\mathrm{d}\Omega_{\hat{n}}\mathrm{d}\Omega_{\hat{k}}} = \frac{4\pi^2\omega^3}{c^3k}\left|\left\langle\Psi_i|\vec{r}\cdot\hat{n}|\Psi^{(+)}_{f,\vec{k}}\right\rangle\right|^2. \tag{2}$$

In the molecular frame, the PICS can be expressed as

$$\frac{\mathrm{d}^2\sigma}{\mathrm{d}\Omega_{\hat{k}}\mathrm{d}\Omega_{\hat{n}}} = \frac{4\pi^2\omega k}{c}|d_{\vec{k},\hat{n}}(\omega)|^2, \tag{3}$$

with

$$d_{\vec{k},\hat{n}}(\omega) = \left(\frac{4\pi}{3}\right)^{1/2}\sum_{lm\mu} d_{lm\mu}Y^*_{lm}(\Omega_{\hat{k}})Y^*_{l\mu}(\Omega_{\hat{n}}) \tag{4}$$

and

$$d_{lm\mu}(\omega) = \left\langle\Psi_i|r_\mu|\Psi^{(-)}_{f,klm}\right\rangle, \tag{5}$$

where the continuum electron wavefunction has been expanded in terms of spherical harmonics, and μ denotes the two components of the light polarization with respect to the molecular frame. For HHG, if the PR process is treated as the inverse of PI, then the returning electron has the momentum along the polarization direction of the harmonics generating laser; thus $\vec{k}$ is parallel to $\hat{n}$. The differential PR and PI cross sections are simply related as seen in equations (1) and (2). In this paper, we will use DPICS mostly when PI and HHG are discussed together.

2.2. Quantitative rescattering theory for high-harmonic generation

According to QRS [19], the laser-induced dipole moment for a fixed-in-space molecule is given by

$$D^{\parallel}(\omega,\theta) = N(\theta)^{1/2}W(\omega)d^{\parallel}(\omega,\theta). \tag{6}$$

Here, we consider the emitted harmonics with polarization parallel to the laser polarization direction only. If needed, the other polarization component can be included straightforwardly [28]. In this equation, ω is the energy of the emitted high-harmonic photon and θ is the angle between the molecular axis and the polarization direction. For simplicity, we only consider linear molecules here. In this equation, $N(\theta)$ is the tunnelling ionization probability of the molecule, which depends on the alignment of the molecule, $W(\omega)$ is the returning electron wave packet. The ionization probability $N(\theta)$ can be calculated using the molecular tunnelling ionization theory (MO-ADK) [29] or the strong field approximation (SFA), while the wave packet can be calculated using the second-order SFA or the so-called Lewenstein model [30]. The PR transition dipole in equation (6) is given by equation (4). Except for $N(\theta)$, all the quantities in equation (6) are complex numbers, each has a magnitude and a phase. More details about the QRS theory for HHG is given in Le *et al* [19].

A few remarks about the QRS in equation (6) are appropriate here. First, it is based on the rescattering model. For atomic targets, its validity has been checked [31] using the laser-induced dipole moment $D^{\parallel}(\omega)$ calculated from the numerical solution of the time-dependent Schrödinger equation (TDSE) and the transition dipole moment $d^{\parallel}(\omega)$ calculated from the PI code. If the continuum wavefunction in the calculation of $d^{\parallel}(\omega)$ is approximated by plane waves, then QRS would reduce to the SFA as given in the Lewenstein model [30]. The tomographic procedure [23–25, 16] is based on this approximation; thus, its validity is very limited.

There is a subtleness in equation (6). For each photon energy ω, the returning electron at a fixed energy is treated as a plane wave while it is at 'infinity'. In HHG, the recombining electron is a localized coherent wave packet, with an angular divergence along the direction of laser polarization. This divergence cannot be included conveniently in equation (6) since in scattering theory, the DPICSs are defined with respect to incident photons with well-defined energies only. Because the wave packet $W(\omega)$ is not directly measurable in an experiment, its independence from the angular spread can be considered as an approximation. It can also be viewed as a conceptual 'wave packet' which is defined to be the proportional constant for each ω in equation (6). In [31], based on TDSE results, $W(\omega)$ has been shown to be independent of the fact whether the target is H or Ne, where the two targets have different angular dependence in the ground state wavefunctions.

2.3. Propagation of high harmonics in the medium

In a typical HHG experiment, a focused laser beam is directed at a gas cell or a gas jet. For impulsively aligned molecules, we will consider harmonics generated at the moment when the molecules are maximally aligned along the polarization direction of the aligning laser. That happens typically near the half-revival. We define an ionization-weighted PR transition dipole moment for each ionization channel j by

$$d^{\mathrm{avg}}(\omega,\alpha) = \int_0^{2\pi}\int_0^{\pi} N(\beta)^{1/2}d^{\parallel}(\omega,\beta)\rho(\theta,\phi)\sin\theta\,\mathrm{d}\theta\,\mathrm{d}\phi. \tag{7}$$

Here α is the angle between the polarization axes of the aligning laser and the probe (or HHG generating) laser and β is the angle between the probing laser and the axis of the fixed-in-space molecules. In this equation, $\rho(\theta,\phi)$ is the angular distribution of the molecules in the probe-laser frame. We consider the possible contributions from different thresholds, j, of the molecular ion. Harmonic signals from multiple orbitals should be obtained by adding the dipoles from equation (7) coherently to obtain $d^{\mathrm{tot}}(\omega,\alpha)$. The high-harmonic signal from each molecule is given by

$$S_h(\omega,\alpha) \propto \omega^4|W(\omega)|^2|d^{\mathrm{tot}}(\omega,\alpha)|^2. \tag{8}$$

To compare with experiments, however, the propagation of the electric field vector generated from all molecules has to be included via the solution of the three-dimensional Maxwell equation

$$\nabla^2 E_h^{\parallel}(r,z,t,\alpha) - \frac{1}{c}\frac{\partial^2 E_h^{\parallel}(r,z,t,\alpha)}{\partial^2 t} = \mu_0 \frac{\partial^2 P_{nl}^{\parallel}(r,z,t,\alpha)}{\partial^2 t}. \tag{9}$$

Here $E_h^{\parallel}(r,z,t,\alpha)$ and $P_{nl}^{\parallel}(r,z,t,\alpha)$ are the parallel components (with respect to the polarization direction of the HHG generating laser) of the electric field of the harmonic, and the nonlinear polarization caused by the IR laser, respectively. Additionally, z is the coordinate of the focused laser beam along the propagation direction and r is perpendicular to it. The nonlinear polarization term is given by

$$P_{nl}^{\parallel}(r,z,t,\alpha) = [n_0 - n_e(r,z,t,\alpha)]D^{\parallel,\mathrm{tot}}(r,z,t,\alpha), \tag{10}$$

where n_0 is the neutral molecule density and $D^{\parallel,\mathrm{tot}}(\omega,\alpha) = W(\omega)d^{\mathrm{tot}}(\omega,\alpha)$ is the averaged induced dipole per aligned molecule multiplied by the returning electron wave packet. These laser-induced dipoles serve as the source for the generation of harmonic fields in equation (9). In equation (10), the electron density n_e at each point in space and time is generated from the tunnelling ionization of the molecules by the laser. Here we assume that only single ionization takes place. If the laser intensity is not too strong and the degree of ionization is small, then the incident fundamental laser field is not modified. When the field is strong, or when the gas pressure is high, the fundamental laser field will be changed during the propagation. In this case, the propagation of the fundamental field must be solved simultaneously with the solution of equation (9) [21].

As shown in Jin *et al* [22], under the condition that the laser intensity is relatively weak and that the gas pressure is not high, the high-order harmonic signal obtained at the detector, which is proportional to $|E_h^{\parallel}(\omega,\alpha)|^2$, can still be expressed as

$$S_h(\omega,\alpha) \propto \omega^4 |W'(\omega)|^2 |d^{\mathrm{tot}}(\omega,\alpha)|^2, \tag{11}$$

where $W'(\omega)$ is the macroscopic wave packet (MWP). In other words, all the effects of propagation, the laser focusing condition, gas pressure effects, etc, are 'dumped' into this term.

Equation (11) relates the experimental HHG spectra to the elementary differential transition dipole matrix elements of individual molecules. Under certain conditions, the latter can be extracted from the measured HHG spectra which can then be compared to DPICS calculations directly. First, if $W'(\omega)$ can be calculated accurately. This can be done if all the experimental parameters are precisely specified, including intensity and spatial and temporal distributions of the focused laser beam and the focusing condition, the gas pressure and how HHG spectra are measured, see Jin *et al* [22]. Second, if the wave packet $W'(\omega)$ is assumed to be 'flat', i.e. independent of ω in the plateau region, as assumed in Shiner *et al* [14]. In this case, $|d^{\mathrm{tot}}(\omega,\alpha)|^2$ is directly proportional to the measured $S_h(\omega,\alpha)$. Third, if an atomic target with similar binding energy is available, and if one can assume that $W'(\omega)$ for the atomic target and the molecular target has the same ω dependence, then $|d^{\mathrm{tot}}(\omega,\alpha)|^2$ for the molecules can be extracted from the known atomic one by comparing the ratio of the HHG spectra. This last approach was used extensively by experimentalists [32, 16, 23, 24]. In doing so, it was assumed that phase matching conditions are satisfied for both targets and for all harmonics. Our numerical simulation has shown that this procedure is quite accurate when the laser intensity is weak and the gas pressure is low [22]. When higher intensity and higher pressure are used in the experiment, the MWP depends on the target (see Wang *et al* [33]). In that case, the comparison method is no longer valid.

3. MFPAD and HHG from aligned N_2 molecules

In this section we apply the theory outlined above to obtain HHG spectra from partially aligned N_2 molecules. In section 3.1, we first show PI cross sections and HHG spectra for a fixed-in-space N_2 molecule. The photon is linearly polarized and the molecular axis makes an angle θ with respect to the polarization direction. Single- and multi-photon ionizations from the highest and next-highest occupied molecular orbitals (HOMO and HOMO-1) are considered. Since molecules cannot be fixed in space, a suitable average over the angular distributions of the partially aligned molecules has to be carried out. For PI, the electrons are generated incoherently; thus the average is carried out incoherently. For HHG, the harmonics are generated by a coherent laser light; thus the averaged induced dipole from the partial aligned molecules has to be calculated coherently, see equation (7). For HHG, the propagation of harmonics in the medium also has to be considered. Section 3.3 illustrates some results of these calculations. Finally, in section 3.4 we address the conditions under which MFPAD, i.e. DPICS, can be extracted from the experimental HHG spectra.

3.1. PI and HHG from fixed-in-space N_2 molecules

High-order harmonics from aligned molecules have been widely investigated over the last few years at different laboratories using 800 nm lasers to 1200–1800 nm NIR lasers. While some measurements reported HHG data for one or two alignment angles, Itatani *et al* [23] and Haessler *et al* [24] had reported HHG spectra over an angular range from 0° to 90° with small steps. In both cases, 800 nm lasers were used.

To illustrate how HHG from aligned N_2 molecules reveals the molecular photoelectron angular distributions, we first look at PI of N_2 by a single photon at 43 eV [11]. We will consider ionization leading to the $X^2\Sigma_g^+$ and $A^2\Pi_u$ states of N_2^+ only. For simplicity, we will use either HOMO and HOMO-1, or σ and π orbitals, to describe these two ionization channels, respectively. We note that single ionization to the $B^2\Sigma_u^+$ state is also important for single PI, but it is not important for HHG due to its higher ionization potential.

In figure 2, we first show theoretical results for total PICS by a photon at 43 eV. The angle θ between the molecular axis and the polarization axis is changed from 0° to 90°. In figure 2(a), the total PICS for both HOMO and HOMO-1 increase with increasing angles, and the two are almost on top of each other. This shows that the total PICS from the HOMO and HOMO-1 at this energy are about the same. In

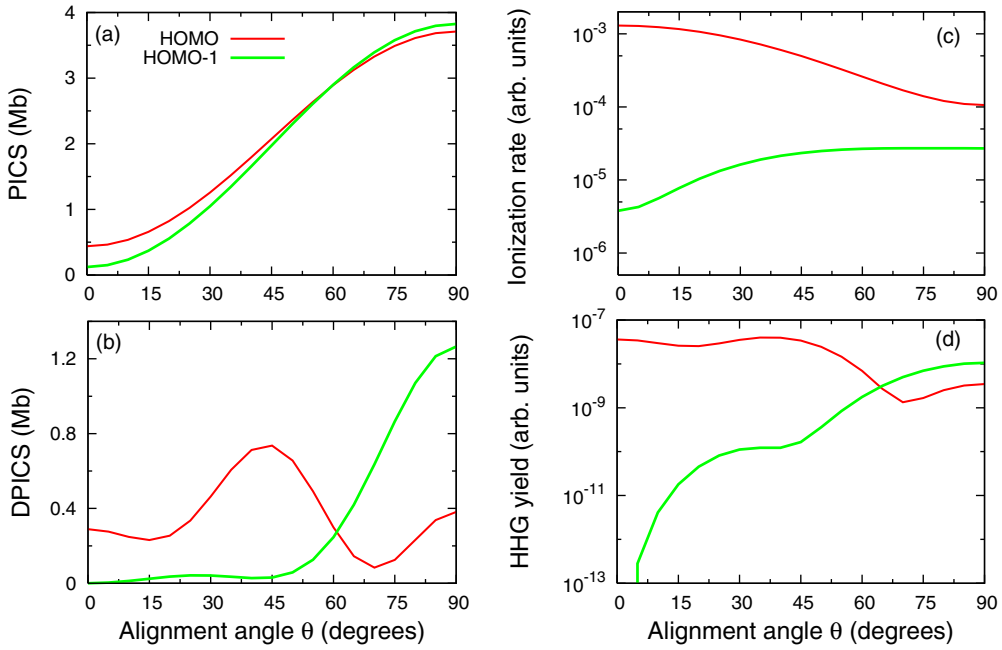

Figure 2. (a) Total PICS and (b) doubly differential cross sections along the laser polarization direction, for N_2 aligned at an angle θ, by a single photon at 43 eV. (c) Alignment dependence of the multi-photon (or tunnelling) ionization rate for N_2 by a laser with intensity of 2×10^{14} W cm^{-2}. (d) Alignment dependence of single-molecule HHG yield (27th order, 43 eV) obtained by using the QRS theory for N_2 exposed to a laser with the intensity of 2×10^{14} W cm^{-2}, wavelength of 800 nm and duration (FWHM) of 30 fs. Reproduced from [11].

figure 2(b), doubly DPICS for electrons along the direction of polarization are shown. They are quite different between the two orbitals. While the HOMO shows the oscillatory structure versus the angle θ, for the HOMO-1 it starts small but increases monotonically with the peak at 90°. This is a clear example of DPICS, or MFPAD, which contains much more detailed information about the molecule which is washed out when integrated over the photoelectron angles, as in the total cross section.

In figure 2(c), multi-photon (or tunnelling) ionization probabilities calculated for a typical laser pulse with the intensity of 2×10^{14} W cm^{-2} and the wavelength of 800 nm are shown. Unlike single PI in figure 2(a), the total multi-photon ionization probability for the HOMO-1 is much smaller than that for the HOMO. At the intensity used in the calculation, tunnelling is the main mechanism for ionization, which decreases exponentially with the ionization potential. Thus, the HOMO-1 is strongly depressed since it lies 1.5 eV deeper than the HOMO. Their alignment dependence is also quite different. Tunnelling, according to the molecular tunneling ionization theory (MO-ADK) [29], depends on the electron density of the molecular orbital along the direction of the laser polarization. Since the HOMO is a σ orbital, its probability peaks at $\theta = 0°$ and has the minimum at 90°. For the HOMO-1, which is a π orbital, the ionization probability is small at θ = 0°, but peaks at 90°. Because of the angular dependence, the ionization probabilities of the HOMO and HOMO-1 may become comparable at or close to θ = 90°. Figure 2(d) shows that HHG from the HOMO-1 overtakes that from the HOMO for θ larger than 50°.

From equation (6), the HHG signal for each fixed-in-space molecule is proportional to the product of tunnelling ionization probability with the DPICS given in figure 2(b). The resulting HHG yields at 43 eV (corresponding to the 27th order harmonic for the 800 nm laser) are shown in figure 2(d) as the angle θ is varied. Note that, as anticipated from equation (6), the HHG yields from each subshell mimic the shape of the DPICS shown in figure 2(b). We comment that tunnelling ionization rates for molecules remain a challenge to calculate accurately [34]. HHG spectra calculated with MO-ADK theory appear to be adequate to interpret the recent HHG spectra for N_2 [35]. In the future, ionization rates for aligned molecules should be determined experimentally together with the HHG spectra.

Figure 2 only shows the spectra at 43 eV. In fact, the amplitude and phase over a range of photon energies are needed for the HHG spectra. In figure 3(a), we compare the DPICS over the 20–80 eV region versus the angle θ between the molecular axis and the polarization axis, for photoelectrons in the direction of the polarization of the light. The corresponding phases of the transition dipole matrix elements are shown in figure 3(b). Recall that these phases will be needed for HHG, since they enter in the laser-induced transition dipole moment for each molecule through equation (6). Similar graphs for the DPICS and the phases for the HOMO-1 are shown in figures 3(c) and (d), respectively. Clearly, both the magnitude and phase change significantly with photon energy and with the angle between the molecular axis and the polarization axis. These elementary DPICS were calculated from the molecular PI code.

To have a closer look at the DPICS calculated from the theory, we display them versus photon energy from 20 to 80 eV, at the interval of $\Delta\theta$ = 15°, for HOMO and HOMO-1, using logarithmic (see figures 4(a) and (b)) scales. For the HOMO,

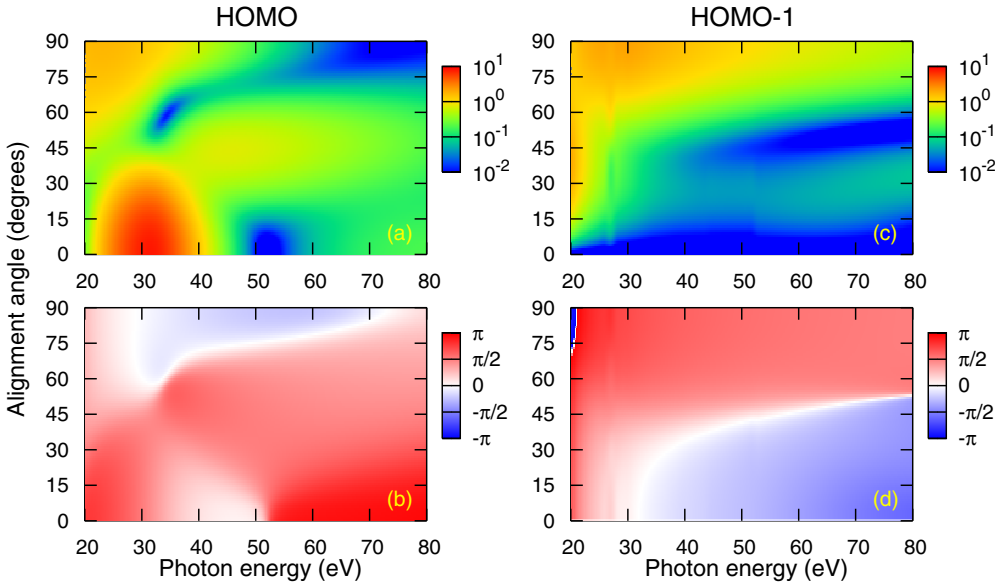

Figure 3. Calculated doubly DPICS ((a) and (c)) and phases ((b) and (d)) (only the parallel component to the polarization direction of the laser) for N_2 as a function of photon energy from the HOMO and HOMO-1. The shape resonance in the HOMO shows up around 30 eV for small alignment angles only. Reproduced from [35]. © 2012 The American Physical Society.

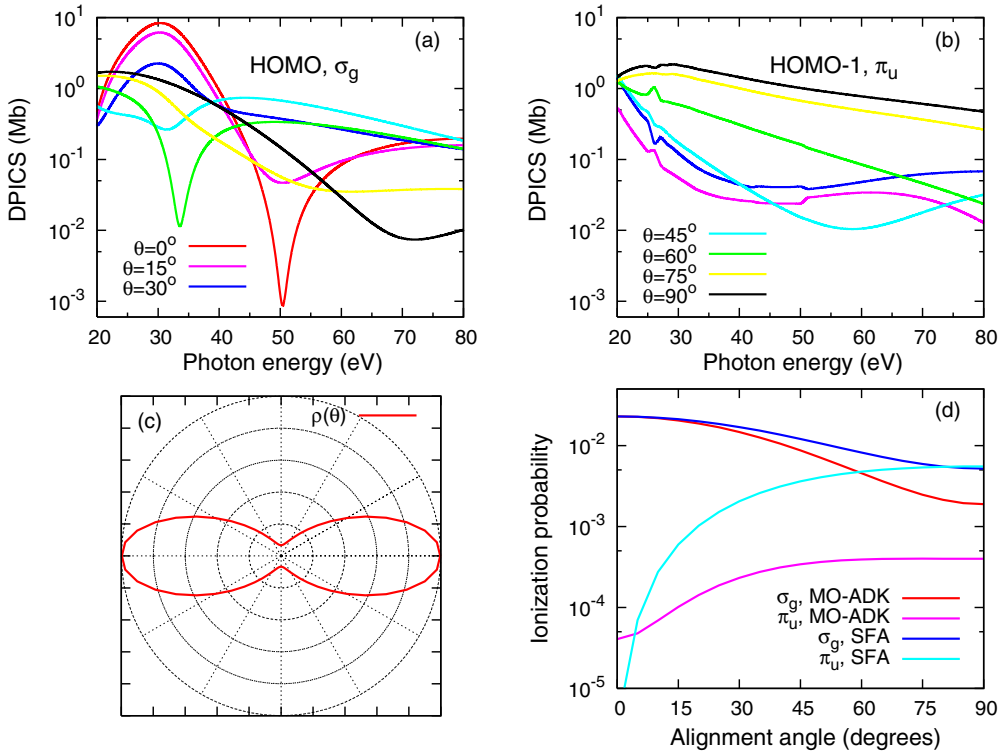

Figure 4. Calculated doubly DPICS along the laser direction of (a) HOMO and (b) HOMO-1 for N_2 as a function of photon energy at the selected alignment angles. These figures are the same as figures 3(a) and (c), but they are only for selected alignment angles. (c) Alignment distribution by an 800 nm aligning laser. Degree of alignment is $\langle \cos^2 \theta \rangle = 0.60$. (d) Alignment-dependent ionization probability calculated by using MO-ADK theory and SFA. Laser parameters: 1.1×10^{14} W cm^{-2}, 1200 nm and 44 fs. The ionization probabilities from MO-ADK and SFA are normalized at alignment angle of 0° for HOMO.

from figure 4(a), the famous shape resonance [26] seen in the total PICS from isotropically distributed N_2 near 20 eV is shown to appear in the DPICS for θ below about 30° only. In fact, in this energy region, the DPICS goes through a minimum near 45°–60°, as can be seen in figure 4(a). Looking at the whole 20–80 eV photon energy region, we note that there is a deep minimum for each fixed θ. At $\theta = 0°$ this occurs at 50 eV. As the angle is increased, the minimum shifts to lower energies, even though it is not clearly visible at 30°. At angles greater than 45°, the position of the minimum shifts to higher

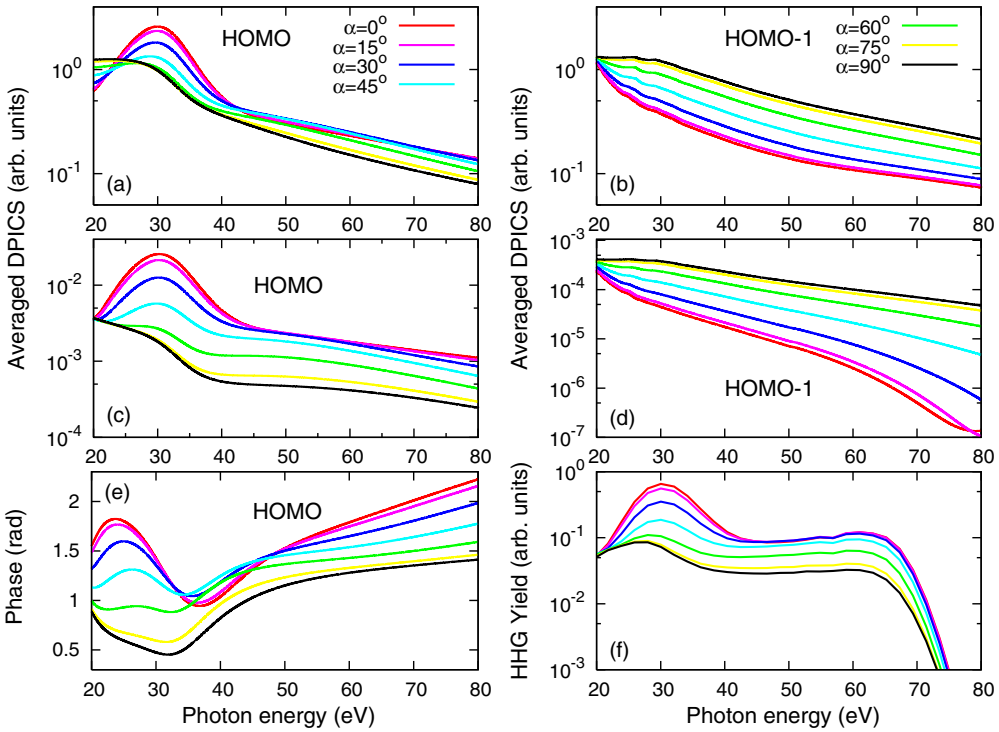

Figure 5. (a), (b) Calculated doubly DPICS in figure 3 averaged over the alignment distribution shown in figure 4(c) at selected pump-probe angle α. (c), (d) Averaged doubly DPICS weighted by alignment-dependent ionization probability according to equation (7) at selected pump-probe angle α. The ionization probability is from figure 4(d) using MO-ADK theory. (e) Phase of averaged PICS in (c) for HOMO. (f) Macroscopic high-harmonic spectra (envelope only) of aligned N_2 including both HOMO and HOMO-1 contributions. Laser parameters: 1.1×10^{14} W cm^{-2}, 1200 nm and 44 fs. Other parameters for macroscopic propagation calculation can be found in [35].

photon energy and the minimum becomes broader. At 90° the minimum occurs at about 70 eV. Near each minimum the phase of the transition dipole matrix element undergoes rapid change with energy (not shown). For the HOMO-1, figure 4(b) shows that the DPICS is larger at large angles. For small θ, the DPICS also show minima, but they are shallower and the magnitudes are smaller in general compared to the HOMO. We point out that the DPICS for the HOMO and HOMO-1 are quite close to each other for angles near 90°. The small kinks in the PI-DCS for the HOMO-1 are probably due to the lack of full convergence in the calculation. These results illustrate that the basic DPICS is quite complicated and they enter in the theory of HHG spectra.

We comment that the minima in DPICS for the HOMO shown in figure 4(a) have been discussed in Le *et al* [19]. These minima change rapidly with the alignment angle and do not follow the pattern predicted by the two-centre interference model [36].

3.2. PI and HHG from partially aligned N_2 molecules

Since molecules cannot be fixed in space, the theoretical predictions in figures 3 and 4(a) and (b) cannot be tested directly in experiments. We consider typical impulsive alignment that can be achieved using 800 nm infrared lasers. Figure 4(c) shows an example of the angular distribution where the molecules are maximally aligned with respect to the aligning laser. Note that the angular distributions in figure 4(c) have cylindrical symmetry with respect to the horizontal axis that is the polarization axis of the aligning laser.

Direct measurements of DPICS from such laser-aligned molecules have begun to appear recently using XUV high-order harmonics generated in atomic gases using 800 nm lasers [10, 12, 13]. Consider molecules that have alignment (or angular) distributions as indicated in figure 4(c). Assume that the polarization axis of the XUV photon makes an angle α with respect to the polarization axis of the aligning laser, we obtain alignment-averaged DPICS for electrons emerging in the polarization direction of the XUV light, and the results are shown in figure 5(a). Compared to figure 4(a), many sharp features predicted for fixed-in-space molecules have been substantially smoothed out, due to limited degrees of alignment. However, the big change of slope near 40 eV for the HOMO channel at small α can be attributed to the minima seen in figure 4(a). The DPICS for the HOMO-1 for different α are shown in figure 5(b). They decrease monotonically with decreasing angle α and with increasing photon energy. The two channels can be separated experimentally in PI measurements since their photoelectron energies differ by 1.5 eV. For PI, the measurement of photoelectron spectra does not provide information on the phase of the transition dipole matrix element versus photon energy. The DPICS for partially aligned molecules were calculated incoherently by averaging over the angular distribution of the molecules.

For HHG from aligned molecules, we first calculate the averaged laser-induced dipole from fixed-in-space molecules coherently at a given laser intensity using equation (7). The equivalent DPICS are shown in figure 5(c). For different angles α, they are more separated due to the additional tunnelling

ionization rates entering equation (7). In fact, the complex amplitudes in equation (7) enter the HHG spectra calculation, not the modulus square. In other words, HHG contains phase information on the transition dipole moment $d^{\parallel}(\omega, \beta)$ which is not available in PI measurements. We comment that the phase of each harmonic can be measured experimentally [37]. In figure 5(e), we show the phase of the complex amplitude in equation (7) from 20 to 80 eV. We note that the phase undergoes a rapid change near the shape resonance at about 25 eV, as well as at around 38 eV for $\alpha = 0^\circ$ to 45°, and at near 32 eV for α from 60° to 90°. We do not show the phases of the transition dipole for the HOMO-1 which does not exhibit interesting features in view of the smoothness of figure 5(d).

Unlike PI, there is no direct method to separate, for example, the contribution of HOMO and HOMO-1 to the HHG. The two amplitudes, each obtained from equation (7), have to be added coherently. The resulting amplitudes are then entered into the propagation equations which can then give the HHG spectra that can be compared to experiments. Figure 5(f) shows an example of the HHG spectra (after propagation) when both HOMO and HOMO-1 contributions are included. Recently we have shown that the HHG theory based on the present QRS model, with the inclusion of the propagation effect, can reproduce experimental HHG spectra for non-aligned N_2 molecules [38], as well as for N_2 aligned at $\alpha = 0^\circ$ [38] and 90° [35]. For such direct comparison between simulation and experiment, detailed information on the experimental conditions is needed. The readers are referred to the original publications for the details mentioned here.

3.3. Probing MFPAD and strong field ionization probabilities using both PI and HHG

We next address how well MFPAD can be probed using PI and HHG for simple molecules. Put more precisely, we ask how well the body-frame dipole matrix elements in equations (1) or (2) can be directly probed by PI or by HHG experiments. For this purpose, PI still has the advantage in general since contributions from different subshells can be distinguished experimentally. On the other hand, as stated previously, the relative phases of the transition dipoles between different photon energies cannot be determined from PI measurements. For HHG, the advantage is that DPICS can be probed over an extended energy region in a single measurement, and the phases of the harmonics reveal the relative phases of the transition dipoles between different photon energies. However, there are disadvantages. First, the contributions from different subshells cannot be easily disentangled in the experiment. Furthermore, tunnelling ionization rates $N(\theta)$ for different subshells are not known accurately. In figure 4(d), we show $N(\theta)$ for the HOMO and HOMO-1 channels, using molecular tunnelling (MO-ADK) theory and the SFA. After normalizing the ionization rate of the HOMO at $\theta = 0^\circ$, figure 4(d) shows that the $N(\theta)$ predicted by MO-ADK and SFA are about the same except near $\theta = 90^\circ$ where the difference is about a factor of 2. For the HOMO-1, while the θ dependence is about the same for the two theories, the absolute values of the HOMO-1 at $\theta = 90^\circ$ differ by about a factor of 10. There are a few reliable calculations or measurements that can provide accurate $N(\theta)$ from different subshells. In Jin *et al* [35], it was shown that the HHG spectra of N_2 at three different intensities can be well reproduced by the simulation using the HOMO and HOMO-1 ionization rates calculated using MO-ADK theory. It would be desirable to check these rates directly in experiments. In the future, a 'complete' experiment probably can include the measurements of photoelectron angular distributions, HHG spectra and total tunnelling ionization probability $N(\theta)$ from partially aligned molecules systematically, including changing the angle α between the alignment axis and the polarization direction of the HHG generating laser (or of the XUV light for PI). Without such an elaborative effort, PI or HHG measurements at most can still only provide partial information on the interaction of photons with molecules, each alone only providing partial knowledge about the molecular system of interest.

4. Summary and perspective

In this paper, we discussed the close connection between molecular-frame photoelectron angular distributions in typical photoionization (PI) experiments and high-order harmonic generation (HHG) by intense lasers. The same theoretically calculated transition dipole matrix elements from fixed-in-space molecules enter in both processes. Since field-free alignment can be achieved using short (about 100 fs) infrared laser pulses, photoionization cross sections and photoelectron spectra can be measured with the XUV harmonics generated by the same laser. By analysing PI and HHG data together, the magnitude and phase of the transition dipole for fixed-in-space molecules can be extracted. Meanwhile, the dependence of the tunnelling ionization rate on the alignment angle between the molecular axis and laser polarization, for highest and next-highest occupied molecular orbital, for example, can also be retrieved from the experimental data. Such experiments together would offer rich information towards a complete understanding of the interaction of molecules with photons. In particular, it would also offer useful experimental data on the most basic quantities such as the alignment-dependent tunnelling ionization rates in strong field physics of molecules. The technology for performing such 'complete' measurements is quickly becoming possible. With enough motivation, perhaps the interaction of photons with molecules can be understood at the most fundamental levels in the near future.

Acknowledgments

This work was supported in part by Chemical Sciences, Geosciences and Biosciences Division, Office of Basic Energy Sciences, Office of Science, US Department of Energy.

References

[1] Bawagan A D and Davidson E R 1999 *Adv. Chem. Phys.* **110** 215
[2] Ueda K 2008 *J. Phys.: Conf. Ser.* **141** 012018
[3] Dill D 1976 *J. Chem. Phys.* **65** 1130

[4] Weber T *et al* 2004 *Nature* **431** 437
[5] Rolles D *et al* 2005 *Nature* **437** 711
[6] Liu X-J *et al* 2008 *Phys. Rev. Lett.* **101** 023001
[7] Stapelfeldt H and Seideman T 2003 *Rev. Mod. Phys.* **75** 543
[8] Pirani F, Cappelletti D, Bartolomei M, Aquilanti V, Scotoni M, Vescovi M, Ascenzi D and Bassi D 2001 *Phys. Rev. Lett.* **86** 5035
[9] Friedrich B and Herschbach D 1999 *J. Phys. Chem.* A **103** 10280
[10] Thomann I, Lock R, Sharma V, Gagnon E, Pratt S T, Kapteyn H C, Murnane M M and Li W 2008 *J. Phys. Chem.* A **112** 9382
[11] Jin C, Le A T, Zhao S F, Lucchese R R and Lin C D 2010 *Phys. Rev.* A **81** 033421
[12] Kelkensberg F, Rouzée A, Siu W, Gademann G, Johnsson P, Lucchini M, Lucchese R R and Vrakking M J J 2011 *Phys. Rev.* A **84** 051404
[13] Rouzée A, Kelkensberg F, Siu W K, Gademann G, Lucchese R R and Vrakking M J J 2012 *J. Phys. B: At. Mol. Opt. Phys.* **45** 074016
[14] Shiner A D, Schmidt B E, Trallero-Herrero C, Wörner H J, Patchkovskii S, Corkum P B, Kieffer J-C, Légaré F and Villeneuve D M 2011 *Nature Phys.* **7** 464
[15] Torres R *et al* 2010 *Opt. Express* **18** 3174
[16] Vozzi C, Negro M, Calegari F, Sansone G, Nisoli M, De Silvestri S and Stagira S 2011 *Nature Phys.* **7** 822
[17] Corkum P B 1993 *Phys. Rev. Lett.* **71** 1994
Krause J L, Schafer K J and Kulander K C 1993 *Phys. Rev. Lett.* **68** 3535
[18] Morishita T, Le A T, Chen Z J and Lin C D 2008 *Phys. Rev. Lett.* **100** 013903
[19] Le A T, Lucchese R R, Tonzani S, Morishita T and Lin C D 2009 *Phys. Rev.* A **80** 013401
[20] Lin C D, Le A T, Chen Z, Morishita T and Lucchese R R 2010 *J. Phys. B: At. Mol. Opt. Phys.* **43** 122001
[21] Jin C, Le A T and Lin C D 2011 *Phys. Rev.* A **83** 023411
[22] Jin C, Le A T and Lin C D 2009 *Phys. Rev.* A **79** 053413
[23] Itatani J, Levesque J, Zeidler D, Niikura H, Pepin H, Kieffer J C, Corkum P B and Villeneuve D M 2004 *Nature* **432** 867
[24] Haessler S *et al* 2010 *Nature Phys.* **6** 200
[25] Haessler S, Caillat and Salieres 2011 *J. Phys. B: At. Mol. Opt. Phys.* **44** 203001
[26] Lucchese R R, Raseev G and McKoy V 1982 *Phys. Rev.* A **25** 2572
Stratmann R E and Lucchese R R 1995 *J. Chem. Phys.* **102** 8493
[27] Werner H-J *et al* 2003 *MOLPRO, Version 2002.6, A Package of Ab Initio Programs* (Birmingham, UK)
[28] Le A T, Lucchese R and Lin C D 2010 *Phys. Rev.* A **82** 023814
[29] Tong X M, Zhao Z X and Lin C D 2002 *Phys. Rev.* A **66** 033402
Zhao S F, Jin C, Le A T, Jiang T F and Lin C D 2010 *Phys. Rev.* A **81** 033423
[30] Lewenstein M, Balcou Ph, Ivanov M Yu, L'Huillier A and Corkum P B 1994 *Phys. Rev.* A **49** 2117
[31] Le A T, Morishita T and Lin C D 2008 *Phys. Rev.* A **78** 023814
[32] Levesque J, Zeidler D, Marangos J P, Corkum P B and Villeneuve D M 2007 *Phys. Rev. Lett.* **98** 183903
[33] Wang G, Jin C, Le A T and Lin C D 2011 *Phys. Rev.* A **84** 053404
[34] Madsen L B, Tolstikhin and Morishita T 2012 *Phys. Rev.* A **85** 053404 and references therein
[35] Jin C, Bertrand J B, Lucchese R R, Wörner H J, Corkum P B, Villeneuve D M, Le A T and Lin C D 2012 *Phys. Rev.* A **85** 013405
[36] Lein M, Hay N, Velotta R, Marangos J P and Knight P L 2002 *Phys. Rev. Lett.* **88** 183903
[37] Mairesse Y *et al* 2003 *Science* **302** 1540
[38] Jin C, Wörner H J, Tosa V, Le A T, Bertrand J B, Lucchese R R, Corkum P B, Villeneuve D M and Lin C D 2011 *J. Phys. B: At. Mol. Opt. Phys.* **44** 095601